Interscale energy transfer in decaying turbulence and vorticity–strain-rate dynamics in grid-generated turbulence

2013 Fluid Dyn. Res. 45 061408

(http://iopscience.iop.org/1873-7005/45/6/061408)

IOP PUBLISHING FLUID DYNAMICS RESEARCH

Fluid Dyn. Res. **45** (2013) 061408 (20pp) doi:10.1088/0169-5983/45/6/061408

Interscale energy transfer in decaying turbulence and vorticity–strain-rate dynamics in grid-generated turbulence

Sylvain Laizet[1], **J C Vassilicos**[1] **and Claude Cambon**[2]

[1] Department of Aeronautics, Imperial College London, London SW7 2AZ, UK
[2] LMFA, Ecole Centrale de Lyon, F-69134 Ecully Cedex, France

E-mail: s.laizet@imperial.ac.uk, j.c.vassilicos@imperial.ac.uk and Claude.Cambom@ec-lyon.fr

Received 27 July 2012, in final form 15 February 2013
Published 27 September 2013
Online at stacks.iop.org/FDR/45/061408

Communicated by K Suga

Abstract

For decaying homogeneous turbulence, we present two assumptions about the energy spectrum and one on the dissipation rate coefficient C_ϵ which, in a high inlet/initial Reynolds number limit, imply that a wide range of wavenumbers exists where the interscale energy flux is dependent on inlet/initial Reynolds number, is negative (kinetic energy is on average transferred from small to high wavenumbers) and is independent of wavenumber but not necessarily of viscosity. Our assumptions about the energy spectrum are not unusual, one concerns the finite nature of the energy and the other its time dependence, and our assumption about C_ϵ is inspired by recent wind tunnel and water channel measurements of turbulence generated by fractal and regular grids. We then present a direct numerical simulation of fractal-generated turbulence where the second-order structure function in time exhibits a well-defined 2/3 power law over more than a decade at a position close to the grid where the local Reynolds number Re_λ is only about 30 and where there is neither average production of enstrophy nor of strain rate. The Q–R and Q_s–R_s diagrams do not have their usual appearance at this position but develop it gradually as the flow progresses downstream and the wide 2/3 power law of the second-order structure function is eroded. It is believed that this is the first time that the spatial development of Q, R, Q_s and R_s statistics is obtained for a spatially developing turbulent flow.

(Some figures may appear in colour only in the online journal)

0169-5983/13/061408+20$33.00

1. Introduction

Recent wind tunnel and water channel experiments by Seoud *et al* (2007), Mazellier and Vassilicos (2010), Valente and Vassilicos (2011, 2012), Gomes-Fernandes *et al* (2012) and Discetti *et al* (2013) have revealed that a substantial region of well-developed decaying turbulence exists in the lee of space-filling fractal square and regular grids where the ratio of the integral length scale L to the Taylor microscale λ remains approximately constant as the turbulence and the Reynolds number $Re_\lambda \equiv \frac{u'\lambda}{\nu}$ decay (u'^2 is a measure of the turbulent kinetic energy and ν is the kinematic viscosity).

Taylor (1935) introduced the dimensionless dissipation constant C_ϵ defined by $\epsilon = C_\epsilon u'^3/L$, where ϵ is the kinetic energy dissipation rate per unit mass. With $\epsilon \sim \nu u'^2/\lambda^2$ (Taylor 1935), it follows that $L/\lambda \sim C_\epsilon Re_\lambda$. The usual assumption that $C_\epsilon = \text{Const}$ at high enough Reynolds number (Batchelor 1953, Townsend 1956, Tennekes and Lumley 1972, Frisch 1995) implies that $L/\lambda \sim Re_\lambda$, i.e. L/λ and Re_λ decay or grow together. The discovery of a substantial region in the lee of some fractal square and regular grids where L/λ remains constant while Re_λ decays implies that $C_\epsilon \sim 1/Re_\lambda$ in that region, in stark contrast with the assumption $C_\epsilon = \text{Const}$ referred to by Tennekes and Lumley (1972) as 'one of the cornerstone assumptions of turbulence theory'. This is a region of well-developed turbulence in the sense that the statistics of turbulent fluctuating velocities (e.g. their streamwise component u) are approximately Gaussian and energy spectra have well-defined power-law shapes with exponents close to $-5/3$ over at least one decade of wavenumbers (see references mentioned above).

Many classical measurements of u' and L along the centreline of various turbulent free shear flows (such as mixing layers and various types of jets and wakes, summarized, for example, in Tennekes and Lumley 1972) can be made to collapse on $L/\lambda \sim Re_\lambda$ if the high Reynolds number assumption is made that $C_\epsilon = \text{Const}$. In fact, this assumption applied to these measurements implies that L/λ and Re_λ have the same dependences on inlet Reynolds number Re_I and streamwise downstream position $x - x_0$, i.e. $L/\lambda \sim R_\text{I}^{1/2} f(\frac{x-x_0}{L_\text{b}})$ and $Re_\lambda \sim R_\text{I}^{1/2} f(\frac{x-x_0}{L_\text{b}})$ with the *same* function f of streamwise position, although f can vary from flow to flow (see Mazellier and Vassilicos 2010, Valente and Vassilicos 2011 for details). The inlet Reynolds number Re_I is based on a characteristic inlet mean flow velocity or mean velocity cross-stream variation U_∞ and on a characteristic cross-stream length scale L_b of the inlet (e.g. a mesh or nozzle of bluff body size), i.e. $Re_\text{I} = \frac{U_\infty L_\text{b}}{\nu}$. The behaviour discovered by Seoud *et al* (2007), Mazellier and Vassilicos (2010), Valente and Vassilicos (2011, 2012), Gomes-Fernandes *et al* (2012) and Discetti *et al* (2013) is very different. What they found is a region of well-developed decaying turbulence that is significantly extended in the streamwise direction and where L/λ is independent of $x - x_0$ even though Re_λ decays with increasing $x - x_0$. They also found that the value of L/λ which remains constant along $x - x_0$ is set by the inlet Reynolds number Re_I and is an increasing function of Re_I as in all boundary-free turbulent flows. Modelling this Re_I-dependence by $L/\lambda \sim Re_\text{I}^{\beta/2}$ ($\beta > 0$) and using the generally valid relation $L/\lambda \sim C_\epsilon Re_\lambda$, their results imply that $C_\epsilon \sim Re_\text{I}^{\beta/2}/Re_\lambda \sim Re_\text{I}^{\beta}/Re_\text{L}$ where $Re_\text{L} = \frac{u'L}{\nu}$. George (1992) had anticipated that L/λ may be independent of local Reynolds numbers Re_λ and Re_L, but nevertheless an increasing function of global Reynolds number Re_I, e.g. proportional to $Re_\text{I}^{1/2}$, about two decades earlier, but for homogeneous decaying turbulence, not specifically for a particular region downstream of fractal square and regular grids.

For more generality and greater sweep of concepts, we introduce one more exponent α and refer to relations such as $C_\epsilon \sim Re_\text{I}^{\beta}/Re_\text{L}^{\alpha}$ ($\alpha, \beta \geqslant 0$) in this paper. Valente and

Vassilicos (2012) find good fits for $\beta = \alpha = 1$ in the flow region mentioned above, but a possibility, of course, remains that these two exponents are not exactly equal to 1 and not necessarily equal to each other either. Batchelor (1953) provides evidence from grid-generated turbulence which seems to suggest that C_ϵ is independent of both Re_l and streamwise distance $x - x_0$, i.e. independent of both global Reynolds number and local turbulence Reynolds number Re_L and therefore $\alpha = \beta = 0$. He interprets this observation as being a 'demonstration that changes in ν which will be accompanied by changes in the motion associated with the dissipation range of wave-numbers, have no effect on the rate of transfer of energy from the lower wavenumbers'.

Note, firstly, that the recently discovered region where both α and β are rather close to 1 is very short and very close to the grid for the particular regular grids which were used to obtain the evidence presented in Batchelor (1953). This region is very significantly lengthened when some fractal grids and some unusual regular grids are used (see Valente and Vassilicos 2012), which explains why it had been missed till 2007 when fractal square grids were introduced for the first time. Secondly, the quote from Batchelor (1953) at the end of the previous paragraph suggests that if $\alpha - \beta \neq 0$, then viscosity may have an effect on the rate of interscale energy transfer at high Reynolds number.

The well-known Richardson–Kolmogorov cascade requires that an intermediate inertial range of wavenumbers exists where the energy flux $\int_0^{k'} T(k)\,\mathrm{d}k$ is negative (i.e. from wavenumbers smaller to wavenumbers larger than k') and independent of both k' and ν (see Batchelor (1953), Sagaut and Cambon (2008) for a definition of the transfer function $T(k)$). This is what Batchelor (1953) is referring to in his quote above. What Kolmogorov proved in this regard for high Reynolds number homogeneous isotropic turbulence by effectively assuming that $\alpha - \beta = 0$ is that an intermediate range of length scales r exists where $\langle \delta u^3(r) \rangle \approx -\frac{4}{5}\epsilon r$ ($\delta u = u(\mathbf{x}+\mathbf{r}) - u(\mathbf{x})$, where u is the fluctuating velocity component in the same direction as $\mathbf{r}$ and the brackets are an average over realizations and/or space $\mathbf{x}$). As shown in Frisch (1995), this relation is equivalent to $\int_0^{k'} T(k)\,\mathrm{d}k \approx -\epsilon$ in the respective intermediate range of wavenumbers and therefore implies the point made by Batchelor (1953), namely 'that changes in ν which will be accompanied by changes in the motion associated with the dissipation range of wave-numbers, have no effect on the rate of transfer of energy from the lower wavenumbers', provided, of course, that $\alpha - \beta = 0$ and ϵ is independent of ν for high enough Reynolds number. In fact, $\int_0^{k'} T(k)\,\mathrm{d}k \approx -\epsilon$ also proves that energy is on average transferred from lower to higher wavenumbers because it implies that $\int_0^{k'} T(k)\,\mathrm{d}k$ is negative. And it also proves that the energy flux $\int_0^{k'} T(k)\,\mathrm{d}k$ is independent of k' in the intermediate range of wavenumbers k' often referred to as inertial equilibrium or simply inertial range. These are central properties of the Richardson–Kolmogorov cascade.

The high Reynolds number scaling $\epsilon \sim u'^3/L$ which results from setting $C_\epsilon = \mathrm{Const}$, i.e. $\alpha = \beta = 0$ (stronger than setting $\alpha - \beta = 0$), is also often seen as a consequence of the Richardson–Kolmogorov cascade's dominance over the mechanism of turbulent energy dissipation because it presupposes that the characteristic time required to dissipate the kinetic energy u'^2 is independent of viscosity and equal to the time needed for the energy to cascade down the scales. The thinking is then that the cascade time can only depend on the remaining fluctuating velocity characteristics, i.e. u' and L, and must therefore be proportional to L/u', thus leading to $\epsilon \sim u'^2/(L/u') = u'^3/L$.

In summary, the universal equilibrium inertial range theory starts from the assumption that $\alpha - \beta = 0$ and then deduces that, in this range, the energy flux is directed towards the smaller scales and is independent of viscosity and scale/wavenumber. This theory is also often used to argue that $\alpha = \beta = 0$. It also imposes dimensional constraints which lead to

the well-known $-5/3$ power-law energy spectrum of turbulent velocity fluctuations in the inertial range. It is important to appreciate that this theory and its consequences are not meant to apply to strictly homogeneous turbulence only. Quoting from Batchelor (1953), 'the statistical quantities determined by the equilibrium range are independent of the properties of the large-scale components of the turbulence and do not require the turbulence to be accurately homogeneous'.

Derivations of $\langle \delta u^3(r) \rangle \approx -\frac{4}{5}\epsilon r$ in an intermediate inertial range of scales r have been proposed for (i) statistically stationary homogeneous isotropic turbulence forced at the large scales (see Frisch 1995), under the high Reynolds number assumption that $C_\epsilon = \text{Const}$, i.e. $\alpha = \beta = 0$; (ii) decaying homogeneous isotropic turbulence (Lundgren 2002, 2003) under the same high Reynolds number assumption that $C_\epsilon = \text{Const}$, i.e. $\alpha = \beta = 0$; and (iii) decaying homogeneous isotropic turbulence by Tchoufag *et al* (2012) under the assumption that the spectral transfer term $T(k)$ is sufficiently small in the assumed inertial range.

In section 2 we offer a re-examination of the assumptions required to obtain cascade properties such as those of the Richardson–Kolmogorov cascade where $\int_0^{k'} T(k)\,\mathrm{d}k$ is negative and independent of both k' and ν in an intermediate range of wavenumbers k'. We show that $T(k)$ is vanishingly small for decaying homogeneous turbulence in an intermediate range of scales under the high Reynolds number assumptions that (i) kinetic energy and its time derivative are finite and that (ii) the ratio of an outer length scale to the Taylor microscale is large enough. We then briefly discuss the consequences of loosening these assumptions and, in particular, how different behaviours of C_ϵ impact on the second assumption concerning the range of scales.

Having obtained $T(k) \to 0$ in a high Reynolds number limit and in a specified range of wavenumbers in section 2, in section 3 we derive $\langle \delta u^3(r) \rangle \approx -\frac{4}{5}\epsilon r$ in a rigorously defined sufficient intermediate range of scales r by using the relation

$$\langle \delta u^3(r) \rangle = 12r \int_0^{+\infty} g_5(kr) T(k)\,\mathrm{d}k \tag{1}$$

of Tchoufag *et al* (2012) where $g_5(kr) = \frac{3(\sin kr - kr\cos kr) - (kr)^2 \sin kr}{(kr)^5}$. Note that this relation relies on large- and small-scale statistical isotropy of the turbulence. Our proof is a rigorous and detailed implementation of the approach first introduced and sketched in Tchoufag *et al* (2012).

The considerations presented in section 2 rely on the Lin equation for homogeneous although not necessarily isotropic turbulence (see Batchelor 1953, Sagaut and Cambon 2008)

$$\frac{\partial}{\partial t} E(k,t) = T(k,t) - 2\nu k^2 E(k,t), \tag{2}$$

which is no more than an energy budget equation ($E(k,t)$ is the turbulence energy spectrum at time t). The derivations that we present in section 2 are no more than the consequences of our assumptions concerning this budget. Our assumptions concern kinetic energy and dissipation and their dependence on Reynolds number, properties which really result from the nonlinear and non-local terms of the Navier–Stokes equations, in particular vorticity and strain-rate dynamics such as vortex stretching and strain-rate amplification (see Tsinober 2009). The spectral transfer term $T(k,t)$ is also strongly influenced by vorticity and strain-rate dynamics, and the formula

$$\frac{\langle \omega \cdot \mathbf{s}\omega \rangle}{\langle \omega^2 \rangle^{3/2}} = \frac{\int_0^\infty k^2 T(k)\,\mathrm{d}k}{(\int_0^\infty k^2 E(k)\,\mathrm{d}k)^{3/2}}, \tag{3}$$

which holds for homogeneous isotropic turbulence (see Batchelor 1953), is but one aspect of the intimate relation between vortex stretching and interscale transfer (ω is the vorticity vector and $\mathbf{s}$ is the strain-rate tensor). In section 4 we present results concerning vorticity, strain and production rates of vorticity and strain obtained from direct numerical simulations (DNS) of grid-generated turbulence. There are statistical inhomogeneities in such turbulent flows and the turbulent fluctuating velocity field $\mathbf{u}$ is a solution of

$$\frac{\partial}{\partial t}\mathbf{u} + \mathbf{u}\cdot\nabla\mathbf{u} = -\nabla p/\rho + \nu\nabla^2\mathbf{u} + \frac{1}{\rho}\mathbf{f}, \tag{4}$$

where

$$\frac{1}{\rho}\mathbf{f} = \mathbf{u}\cdot\nabla\overline{\mathbf{u}} + \frac{\partial}{\partial x_k}\langle u_k\mathbf{u}\rangle - \overline{\mathbf{u}}\cdot\nabla\mathbf{u} \tag{5}$$

in terms of the mean flow field $\overline{\mathbf{u}}$, the turbulent fluctuating pressure p and the fluid density ρ (these equations result from a Reynolds decomposition applied to the Navier–Stokes equation and the brackets symbolize an average over time). In section 4 we report on properties of the vorticity and strain rate of the fluctuating velocity, i.e. $\omega \equiv \nabla\times\mathbf{u}$ and $s_{ij} \equiv \frac{1}{2}(\frac{\partial}{\partial x_i}u_j + \frac{\partial}{\partial x_j}u_i)$, in spatially developing grid-generated turbulent flows.

2. The interscale energy flux

We focus in this section on decaying homogeneous turbulence. Integrating the Lin equation and making use of the total energy $K = \int_0^{+\infty} E(k,t)\,\mathrm{d}k$ and the total energy dissipation rate $\epsilon = 2\nu\int_0^{+\infty} k^2 E(k,t)\,\mathrm{d}k$, we obtain that

$$\frac{\mathrm{d}}{\mathrm{d}t}K = \int_0^{+\infty} T(k,t)\,\mathrm{d}k - \epsilon. \tag{6}$$

As energy is lost only by dissipation from viscous forces in homogeneous turbulence, i.e. $\frac{\mathrm{d}}{\mathrm{d}t}K = -\epsilon$,

$$\int_0^{+\infty} T(k,t)\,\mathrm{d}k = 0. \tag{7}$$

We now explore the consequences of the following first assumption: an outer length scale $l_\mathrm{o}(t)$ exists which is such that, for $k' l_\mathrm{o} \gg 1$,

$$\int_0^{k'} E(k,t)\,\mathrm{d}k \approx K \tag{8}$$

(assumption 1a) and

$$\int_0^{k'} \frac{\partial}{\partial t}E(k,t)\,\mathrm{d}k \approx -\epsilon \tag{9}$$

(assumption 1b).

Integrating the Lin equation (2) from $k = 0$ to k' and applying assumption 1b yields

$$-\epsilon \approx \int_0^{k'} T(k,t)\,\mathrm{d}k - 2\nu\int_0^{k'} k^2 E(k,t)\,\mathrm{d}k. \tag{10}$$

Note that $2\nu\int_0^{k'} k^2 E(k,t)\,\mathrm{d}k < 2\nu k'^2\int_0^{k'} E(k,t)\,\mathrm{d}k$ and that, on the basis of assumption 1a, $2\nu k'^2\int_0^{k'} E(k,t)\,\mathrm{d}k \approx 2\nu k'^2 K$ (assumption 1a is effectively that K is finite which would,

alternatively, allow us to use $2\nu k'^2 \int_0^{k'} E(k,t)\,\mathrm{d}k \leqslant 2\nu k'^2 K < \infty$ without changing our conclusions). The term $2\nu \int_0^{k'} k^2 E(k,t)\,\mathrm{d}k$ in (10) can then be neglected compared to ϵ if $\epsilon \gg 2\nu k'^2 K$ and it can then be concluded that

$$-\epsilon \approx \int_0^{k'} T(k,t)\,\mathrm{d}k \tag{11}$$

in the range $l_\mathrm{o}^{-1} \ll k' \ll (\frac{\epsilon}{2\nu K})^{1/2}$, provided, of course, that such a range exists, which it does if

$$l_\mathrm{o} \gg \left(\frac{2\nu K}{\epsilon}\right)^{1/2}. \tag{12}$$

The consequence of our assumptions and of (12) is that the interscale energy flux $\int_0^{k'} T(k,t)$ is negative and is also independent of k' in the range $l_\mathrm{o}^{-1} \ll k' \ll (\frac{\epsilon}{2\nu K})^{1/2}$. This is very much like the Richardson–Kolmogorov cascade where $\int_0^{k'} T(k,t)$ is negative (energy cascades down the scales) and independent of k' (at a constant interscale energy flux) in the inertial range. However, the range $l_\mathrm{o}^{-1} \ll k' \ll (\frac{\epsilon}{2\nu K})^{1/2}$ is not the usual inertial range because it does not involve the Kolmogorov microscale. It does, however, involve the Taylor microscale $\lambda \sim (2\nu K/\epsilon)^{1/2}$. We stress that our analysis does not lead to the Kolmogorov microscale which would require further arguments, usually of a phenomenological nature.

The scaling of λ^{-1} is determined by the scaling of ϵ. Our second assumption is that $C_\epsilon \equiv \epsilon L/K^{3/2}$ scales similarly to the general way indicated by the grid-generated turbulence experiments in the introduction, i.e. (assumption 2)

$$C_\epsilon \sim Re_\mathrm{L}(0)^\beta / Re_\mathrm{L}^\alpha, \tag{13}$$

where $\alpha, \beta \geqslant 0$, $Re_\mathrm{L} = Re_\mathrm{L}(t) \sim K^{1/2}L/\nu$ and where this Reynolds number at time $t = 0$ plays the role of the inlet Reynolds number Re_I in grid-generated turbulence. Hence the range $l_\mathrm{o}^{-1} \ll k' \ll \lambda^{-1}$ becomes

$$l_\mathrm{o}^{-1} \ll k' \ll L^{-1} Re_\mathrm{L}(0)^{\beta/2} Re_\mathrm{L}^{(1-\alpha)/2}. \tag{14}$$

It is natural to expect $l_\mathrm{o} \sim L$, in which case $Re_\mathrm{L}(0)^{\beta/2} Re_\mathrm{L}^{(1-\alpha)/2} \gg 1$ is enough to imply that this wavenumber range exists and is wide. This range and $Re_\mathrm{L}(t)$ decrease with time together when $\alpha < 1$. However, when $\alpha = 1$ this range remains constant as $Re_\mathrm{L}(t)$ decreases, which is close to the new regime observed by Seoud *et al* (2007), Mazellier and Vassilicos (2010), Valente and Vassilicos (2011, 2012), Gomes-Fernandes *et al* (2012) and Discetti *et al* (2013) as mentioned in the introduction.

The mechanism responsible for (13) in this section's setting or for $C_\epsilon \sim Re_\mathrm{I}^\beta / Re_\mathrm{L}^\alpha$ in grid-generated turbulence is also responsible, when $Re_\mathrm{L}(0)^{\beta/2} Re_\mathrm{L}^{(1-\alpha)/2} \gg 1$, for the existence and breadth of the wavenumber range (14). This mechanism must somehow depend on the flow dynamics near the inlet/initial conditions judging from the presence of $Re_\mathrm{L}(0)$ in formula (13). In turn, the existence of such a broad range directly implies a forward cascade of the type (11) if (8) and (9) hold at $k' l_\mathrm{o} \gg 1$. However, this cascade may be viscosity dependent as this is not a range where the interscale energy flux is independent of viscosity except in the particular case where $\alpha = \beta$ because of $C_\epsilon \sim \frac{Re_\mathrm{L}(0)^\beta}{Re_\mathrm{L}^\alpha}$.

In conclusion, the picture that emerges from the adoption of assumptions 1 and 2 is that something may happen near the inlet/initial conditions causing assumption 2 to materialize and that if this happens with a sufficiently high inlet/initial Reynolds number and $\alpha \leqslant 1$, then $Re_\mathrm{L}(0)^{\beta/2} Re_\mathrm{L}^{(1-\alpha)/2}$ is large enough to immediately ensure the existence of a wide

range of wavenumbers where energy cascades down the scales at a rate ϵ. This cascade will persist for as long as $Re_L(t)$ is large enough to keep $Re_L(0)^{\beta/2} Re_L^{(1-\alpha)/2} \gg 1$ and it is such that the interscale energy flux is independent of wavenumber but not necessarily of viscosity. Unlike the usual Richardson–Kolmogorov cascade, this flux depends on inlet/initial conditions through its dependence on $Re_L(0)$ or Re_I.

An immediate consequence of our conclusion is the converse statement that if $Re_L(0)^{\beta/2} Re_L^{(1-\alpha)/2}$ is large enough for assumptions 2 and 1a to imply the existence of the wide range of wavenumbers $l_o^{-1} \ll k' \ll (\frac{\epsilon}{2\nu K})^{1/2}$ but the interscale energy flux does not equal $-\epsilon$ in that range, then assumption 1b must be wrong. This is an eventuality which would invalidate the usual attempts to obtain the Kolmogorov energy spectrum from dimensional arguments based on the interscale energy flux because it would imply that the rate of kinetic energy loss does not equal that flux. As a result, the dimensional analysis would need to consider two independent variables with the same dimensions ($\int_0^{k'} T(k,t)\,\mathrm{d}k$ and ϵ), one of which would not be guaranteed to be independent of k and would therefore not be able to imply $E(k) \sim k^{-5/3}$ and, equivalently, $\langle \delta u^2(r) \rangle \sim r^{2/3}$ in the appropriate ranges of scales without additional assumptions.

In section 4, alongside our study of velocity gradient invariants which underpin fundamental dissipation properties, we also offer a preliminary test of the idea that the existence of two widely separated length scales (one large/outer and one small/inner) may precede and perhaps even contribute to the appearance of a $k^{-5/3}$ energy spectrum. We do this in a grid-generated turbulent flow as this is where dissipation laws such as (13) have been discovered so far. The turbulence in these flows is inhomogeneous and anisotropic near the grid and so we are transferring an idea which came out of our study of decaying homogeneous turbulence in this section to inhomogeneous turbulence in section 4.

In the following section, we show how to obtain $\langle \delta u^3(r) \rangle \approx -\frac{4}{5}\epsilon r$ for decaying homogeneous isotropic turbulence from the results derived in this section on the basis of assumptions 1 and 2. We leave the generalization of this derivation to homogeneous not strictly isotropic turbulence for a future study.

3. The third-order structure function

We pick two wavenumbers k_o and k_i such that $l_o^{-1} \ll k_o \ll k_i \ll l_i^{-1}$ where $l_i \sim \lambda$ and decompose equation (1), which holds for strictly homogeneous isotropic turbulence, into three terms as follows:

$$\frac{\langle \delta u^3(r) \rangle}{12r} = \int_0^{k_o} g_5(kr) T(k)\,\mathrm{d}k + \int_{k_o}^{k_i} g_5(kr) T(k)\,\mathrm{d}k + \int_{k_i}^{+\infty} g_5(kr) T(k)\,\mathrm{d}k. \tag{15}$$

For separations $r \ll k_o^{-1}$, $g_5(kr) \approx 1/15$ for any $k \leqslant k_o$, which means that

$$\int_0^{k_o} g_5(kr) T(k)\,\mathrm{d}k \approx \frac{1}{15} \int_0^{k_o} T(k)\,\mathrm{d}k. \tag{16}$$

In the limit $Re_L(0)^{\beta/2} Re_L^{(1-\alpha)/2} \gg 1$ and for $k_o l_o \gg 1$ under assumptions 1 and 2, we have seen that $\int_0^{k_o} T(k)\,\mathrm{d}k \approx -\epsilon$ for strictly homogeneous isotropic turbulence. Hence,

$$\int_0^{k_o} g_5(kr) T(k)\,\mathrm{d}k \approx -\epsilon/15 \tag{17}$$

in this limit and for $rk_o \ll 1$.

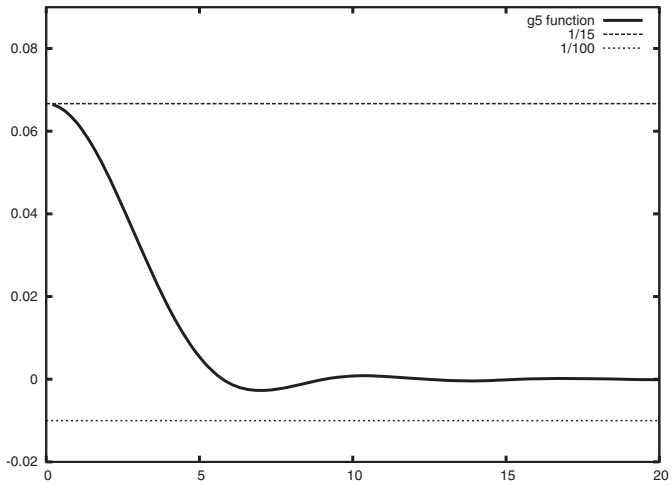

Figure 1. Plot of the function g_5 appearing in equation (1) against kr.

Now for the second term $\mathrm{ST} \equiv \int_{k_o}^{k_i} g_5(kr)T(k)\,\mathrm{d}k$, we define $T_+ \equiv \sup[T(k), 0]$ and $T_- \equiv \inf[T(k), 0]$ and note that

$$\mathrm{ST} = \mathrm{ST}_+ + \mathrm{ST}_-, \tag{18}$$

where $\mathrm{ST}_+ \equiv \int_{k_o}^{k_i} g_5(kr)T_+(k)\,\mathrm{d}k$ and $\mathrm{ST}_- \equiv \int_{k_o}^{k_i} g_5(kr)T_-(k)\,\mathrm{d}k$. The function $g_5(kr)$ is such that $-\frac{1}{100} < g_5(kr) \leqslant \frac{1}{15}$ (see figure 1); hence

$$-\frac{1}{100}\int_{k_o}^{k_i} T_+(k)\,\mathrm{d}k < \mathrm{ST}_+ \leqslant \frac{1}{15}\int_{k_o}^{k_i} T_+(k)\,\mathrm{d}k \tag{19}$$

and

$$-\frac{1}{15}\int_{k_o}^{k_i} T_-(k)\,\mathrm{d}k < \mathrm{ST}_- \leqslant \frac{1}{100}\int_{k_o}^{k_i} T_-(k)\,\mathrm{d}k. \tag{20}$$

We have seen that $T(k) \to 0$ in $l_o^{-1} \ll k \ll l_i^{-1}$ in the limit $Re_L(0)^{\beta/2}Re_L^{(1-\alpha)/2} \gg 1$, i.e. $T_+(k)$ and $T_-(k)$ are also vanishingly small in that same range and limit. We can therefore expect the upper and lower bounds of ST_+ and ST_- to tend to 0 in the limit $Re_L(0)^{\beta/2}Re_L^{(1-\alpha)/2} \gg 1$, which leaves us with

$$\int_{k_o}^{k_i} g_5(kr)T(k)\,\mathrm{d}k \approx 0 \tag{21}$$

for any r as long as $Re_L(0)^{\beta/2}Re_L^{(1-\alpha)/2} \gg 1$ and $l_o^{-1} \ll k \ll l_o^{-1}$.

We must finally treat the third and final term, $\int_{k_i}^{+\infty} g_5(kr)T(k)\,\mathrm{d}k$. This term is approximately equal to $-\int_{k_i}^{+\infty} \frac{\sin(kr)}{(kr)^3}T(k)\,\mathrm{d}k$ in the limit $rk_i \gg 1$. Hence, it can be written as

$$-\frac{1}{(k_i r)^3}\int_{k_i}^{+\infty} \frac{\sin(kr)}{(k/k_i)^3}T(k)\,\mathrm{d}k \tag{22}$$

which tends to 0 in the limit $rk_i \gg 1$.

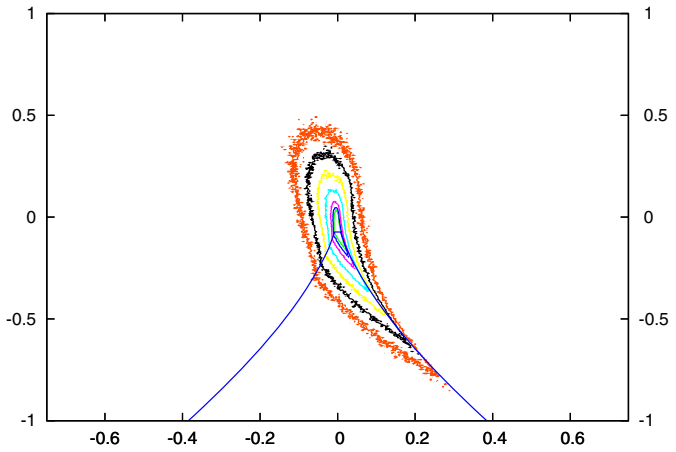

Figure 2. Q–R diagram obtained from a DNS of periodic statistically stationary turbulence (courtesy of Dr R Onishi, see Onishi *et al* (2011) for details of this DNS). The vertical/horizontal axes are for $Q/\langle \mathrm{tr}(\mathbf{s}^2)\rangle$ and $R/\langle \mathrm{tr}(\mathbf{s}^2)\rangle^{3/2}$, respectively, and the plot is of isovalues of the probability density function of (Q, R) (we use seven different colours for seven different isovalues between 0.4 for green and 0.0125 for orange. The same isovalues are used for the same colours in figures 6–19). In the case of this DNS the statistics are taken over all space for a single time shot.

Putting together these three asymptotic behaviours of the three terms adding up to $\frac{\langle \delta u^3(r)\rangle}{12r}$, we are left with the following first-order asymptotic result as $Re_{\mathrm{L}}(0)^{\beta/2} Re_{\mathrm{L}}^{(1-\alpha)/2} \to \infty$:

$$\frac{\langle \delta u^3(r)\rangle}{12r} \approx -\epsilon/15 \tag{23}$$

in the range $k_{\mathrm{i}}^{-1} \ll r \ll k_{\mathrm{o}}^{-1}$. This range increases as $Re_{\mathrm{L}}(0)^{\beta/2} Re_{\mathrm{L}}^{(1-\alpha)/2} \to \infty$ because $l_{\mathrm{o}}/l_{\mathrm{i}} \to \infty$ in that limit so that there is more and more room for $k_{\mathrm{i}}/k_{\mathrm{o}}$ to grow towards infinity too.

This concludes our derivation of the $-4/5$ law

$$\langle \delta u^3(r)\rangle \approx -\frac{4}{5}\epsilon r \tag{24}$$

for decaying homogeneous isotropic turbulence in the appropriate intermediate range of scales r and the appropriate Reynolds number limit under assumptions 1 and 2.

4. DNS of turbulent flows generated by a fractal square grid

Assumptions about turbulence dissipation (such as assumptions 1 and 2) and their consequences for interscale energy transfer are reflections of deeper turbulence dynamics involving vorticity and strain-rate interactions. Indeed, $\epsilon = 2\nu\langle \mathrm{tr}(\mathbf{s}^2)\rangle$, and $T(k)$ is closely related to vortex stretching, for example via (3) in homogeneous isotropic turbulence. One way to obtain some insight into turbulence vorticity and strain rate statistics is in terms of the Q–R diagram (Tsinober 2009) where $Q \equiv \frac{1}{4}(\omega^2 - 2\,\mathrm{tr}\,\mathbf{s}^2)$ and $R \equiv -\frac{1}{3}(s_{ij}s_{jk}s_{ki} + \frac{3}{4}\omega_i s_{ij}\omega_j)$. This diagram has the tear drop shape shown in figure 2 in many turbulent flows: turbulent boundary layers, mixing layers, grid turbulence, jet turbulence (see Tsinober 2009). This has led Tsinober (2009) to advance the idea that this tear drop shape may be one of the qualitatively universal features of turbulent flows. This potentially universal tear drop is such

that points in the flow dominated by strain rather than vorticity, i.e. regions where $Q < 0$, are also regions where the production rate of $\frac{1}{2}\mathrm{tr}(\mathbf{s}^2)$ is greater than the production rate of $\frac{1}{4}\omega^2$, i.e. regions where $R > 0$.

To the best of our knowledge, there are no data in the literature on the spatial development of the Q–R diagram in spatially developing turbulent flows, either from laboratory experiments or from computer simulations. The picture suggested by our analysis in section 2 is one where, at high enough inlet Reynolds number and relatively close to the inlet of a grid-generated turbulence, a flow phenomenon may occur which is linked to a dependence of dissipation on Reynolds numbers such as $C_\epsilon \sim Re_\mathrm{I}^\beta / Re_\mathrm{L}^\alpha$ and directly causes a wide separation between outer and inner scales. This then induces a particular type of cascade (rather than the other way around) which persists for a significant distance downstream and at most as long as the local Reynolds number has not decayed too much. An energy cascade towards the small scales implies a positive value of $T(k)$ at very high wavenumbers (see equation (7)), which in turn implies a positive value of $\langle \omega_i s_{ij} \omega_j \rangle$ in homogeneous isotropic turbulence by direct application of (3). For homogeneous/periodic turbulence, it can also be proven that $\langle Q \rangle = 0$ and $\langle R \rangle = 0$ (Batchelor 1953, Tsinober 2009). Hence the production rate of $\frac{1}{2}\,\mathrm{tr}\,\mathbf{s}^2$, namely $-s_{ij}s_{jk}s_{ki} - \frac{1}{4}\omega_i s_{ij}\omega_j$, is on average equal to the production rate of $\frac{1}{4}\omega^2$, namely $\frac{1}{2}\omega_i s_{ij}\omega_j$, and for a forward cascade both these averages are positive, i.e. $\langle -s_{ij}s_{jk}s_{ki} - \frac{1}{4}\omega_i s_{ij}\omega_j \rangle = \frac{1}{2}\langle \omega_i s_{ij}\omega_j \rangle > 0$ (see Tsinober 2009). The Q–R diagram's tear-drop shape adds the information that the production rate of $\frac{1}{2}\,\mathrm{tr}\,\mathbf{s}^2$ is nevertheless greater than the production rate of $\frac{1}{4}\omega^2$ at those places where $Q < 0$.

It is therefore meaningful to investigate how the statistics of $\omega_i s_{ij} \omega_j$ and $s_{ij}s_{jk}s_{ki}$ develop downstream of a turbulence-generating grid if we want to acquire some insight into how a cascade is set off, with what properties it is set off, how these properties evolve and whether this happens before or after the appearance of a wide range of excited length scales. We address this question by a DNS of grid-generated turbulence and offer results on the streamwise evolution of the Q–R diagram and of averages of ω^2, $\mathrm{tr}\,\mathbf{s}^2$, $\omega_i s_{ij}\omega_j$ and $s_{ij}s_{jk}s_{ki}$ in spatially developing flows.

We consider two turbulence-generating grids, one regular and one fractal (see figure 3) of the same blockage ratio $\sigma = 0.507$ (the ratio of the area blocked by the grid to the area T^2 of the channel/tunnel square section), the same thickness in the streamwise direction (normal to the grid) and the same effective mesh size $M_\mathrm{eff} = \frac{4T^2}{L_\mathrm{G}}\sqrt{1-\sigma}$, where L_G is the total length of the grid when it has been stripped of its thickness (Hurst and Vassilicos 2007). The concept of an effective mesh size was defined and introduced by Hurst and Vassilicos (2007) and given an interpretation in terms of the turbulent flow by Laizet and Vassilicos (2012); in the case of regular grids, M_eff equals M, the actual mesh size (see figure 3). The fractal grid is a four-iteration space-filling fractal square grid with thickness ratio $t_r = 8.5$ (see figure 3 and Hurst and Vassilicos (2007) for definitions of 'space filling' and t_r).

4.1. Flow parameters and numerical method

Each grid is placed in a computational domain with streamwise length L_x and spanwise extents $L_y = L_z = T$. For the fractal grid, $L_x = 1152t_\mathrm{min}$ and $T = 144t_\mathrm{min}$ where t_min is the spanwise thickness of the smallest bars on the grid (see figure 3). For the regular grid, $L_x = 576b$ and $T = 36b$ where b is the spanwise thickness of the bars on the grid (see figure 3). The streamwise thickness of both grids is $3t_\mathrm{min}$ and the boundary layers are laminar at the grid, resulting in boundary layer thicknesses smaller than $0.5t_\mathrm{min}$; also $b = 2t_\mathrm{min}$ and $M_\mathrm{eff} = 6.5t_\mathrm{min}$.

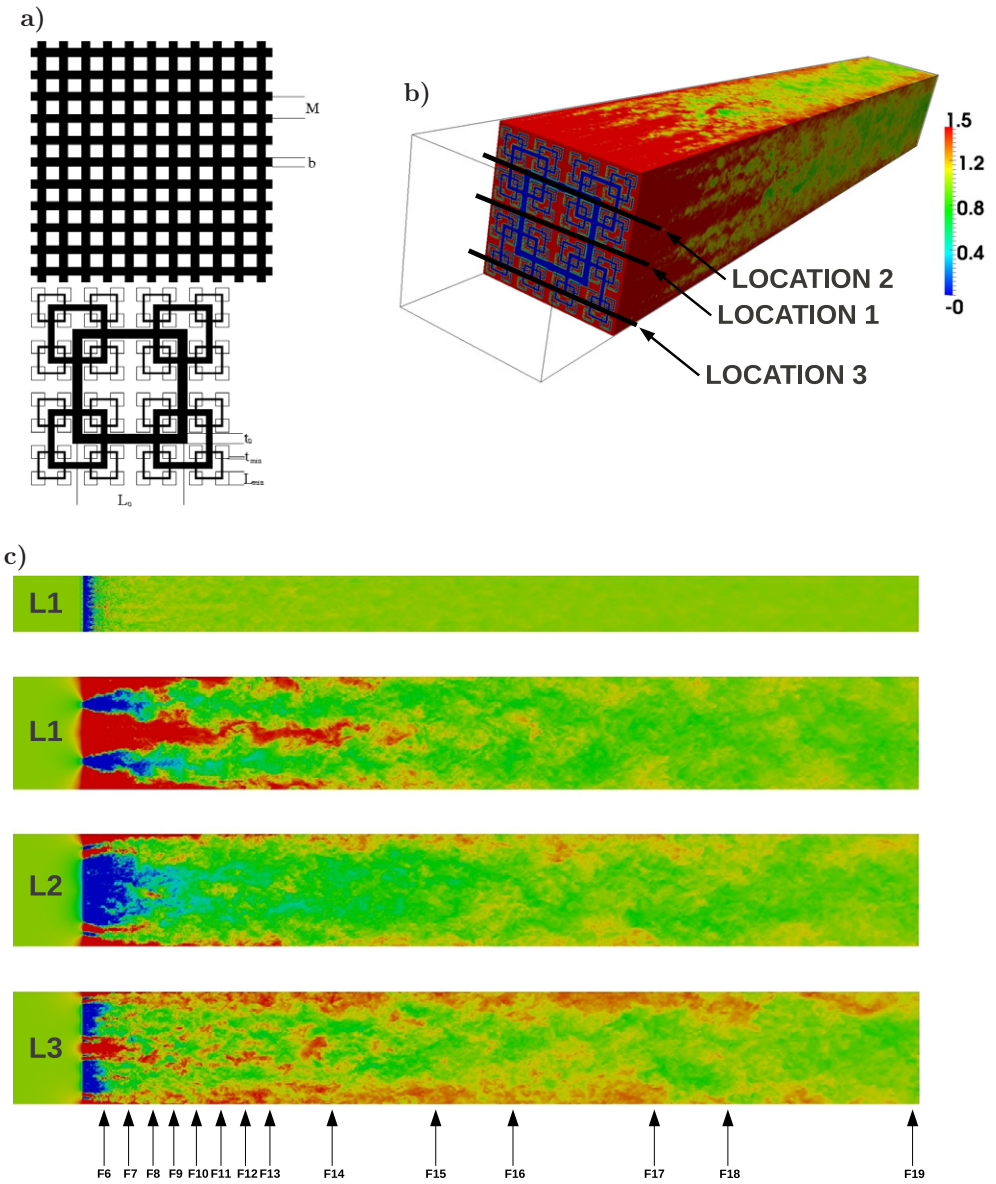

Figure 3. (a) Regular (mesh size M and bar thickness b) and fractal monoplanar grids of the same σ, M_{eff} and streamwise thickness. Four iterations of bar lengths $L_n = 2^{-n}T/2$ ($L_{\min} = L_3$) and thicknesses $t_n = (2.041)^{3-n}t_{\min}$, $n = 0, 1, 2, 3$ on the fractal grid. (b) Three-dimensional (3D) visualization of a computational domain with grids and a downstream streamwise velocity field. (c) Two-dimensional (2D) (x, y) cuts through the streamwise velocity field. Top, for regular grid. Then locations 1,2,3 for fractal grid where different size wakes are visible. The locations corresponding to figures 6–19 are indicated as F6–F19. In all these plots, the colours are gradations of the streamwise fluid velocity component in units where $U_\infty = 1$.

We assume a fluid of uniform density and kinematic viscosity ν and inflow/outflow boundary conditions in the streamwise direction with a uniform fluid velocity U_∞ without turbulence as inflow condition and a one-dimensional convection equation as outflow

condition. The boundary conditions in the two spanwise directions are periodic. Defining $\mathbf{x} \equiv (x, y, z)$ to be spatial coordinates in the streamwise (x) and two spanwise directions, the inflow is at $x = -14M_{\text{eff}}$ and the grid is placed at $x = 0$. The inlet Reynolds number $Re_{\text{I}} \equiv \frac{U_\infty M_{\text{eff}}}{\nu}$ is 1950 for both the grid cases. Our initial condition for the velocity field is $\mathbf{u} \equiv (u, v, w) = (U_\infty, 0, 0)$ everywhere (u is the streamwise velocity component and (v, w) are the two spanwise velocity components corresponding to (y, z)).

We solve the incompressible Navier–Stokes equations on a Cartesian mesh with our numerical code Incompact3d which is based on sixth-order compact schemes for spatial discretization and a third-order Adams–Bashforth scheme for time advancement. To treat the incompressibility condition, a fractional step method requires solving a Poisson equation. This equation is fully solved in spectral space, via the use of relevant 3D fast Fourier transforms (FFTs). The pressure mesh is staggered from the velocity mesh by half a mesh, to avoid spurious pressure oscillations. With the help of the concept of modified wave number, the divergence-free condition is ensured up to machine accuracy. The modelling of the grids is performed by an immersed boundary method, following a procedure proposed by Parnaudeau *et al* (2008). The present method is a direct forcing approach that ensures the no-slip boundary condition at the grid walls. It mimics the effects of a solid surface on the fluid with an extra forcing in the Navier–Stokes equations. Full details of the code, its validations and its application to grid-generated turbulence can be found in Laizet and Lamballais (2009) and Laizet and Vassilicos (2011).

In terms of the Kolmogorov microscale η (the smallest length scale of the turbulence), the spatial resolution is at worst $\Delta x = \Delta y = \Delta z = 4\eta$ for the fractal grid and 8η for the regular grid (where the turbulence is at its most intense and $\eta \approx 0.125t_{\text{min}}$ for the fractal grid and $\approx 0.0625t_{\text{min}}$ for the regular grid) and at best $\Delta x = \Delta y = \Delta z = \frac{4}{3}\eta$ for the fractal grid and $\frac{7}{4}\eta$ for the regular grid (at the end of the computational domain where the turbulence has decayed and $\eta \approx 0.375t_{\text{min}}$ for the fractal grid and $\approx 0.286t_{\text{min}}$ for the regular grid). The time step is $0.01t_{\text{min}}/U_\infty$ (low enough for the CFL to be 0.75) and resolves the smallest time scales of our flows which are η/U_∞. Statistics are collected and averages taken over 125 000 time steps at various points in the flow along the centreline normal to either grid; and along a line normal to the fractal grid and crossing its biggest bar at the middle.

For the fractal grid flow the Cartesian mesh has 2881 nodes in the streamwise direction and 360×360 nodes in the other two directions, i.e. about 374 million mesh nodes in total, and is split into 8100 computational cores. For the regular grid flow, the Cartesian mesh has 2881 nodes in the streamwise direction but 180×180 nodes in the other two directions, i.e. about 93 million mesh nodes in total, and is split into 7200 computational cores. The size of the present simulations are such that we have no alternative but to use the parallel version of this code (Laizet and Li 2011). Based on a highly scalable 2D decomposition library and a distributed FFT interface, it is possible to use the code on thousands of computational cores (more details of this efficient parallel strategy can be found in Laizet and Li 2011). We ran it on HECToR's Cray XE6 system (based on six-core processors; HECToR is the UK's national supercomputing facility).

4.2. DNS results

Figures 3(b) and (c) illustrate our two turbulent flows including snapshots of instantaneous streamwise velocity fields at the different (x–y) planes. For the fractal grid, there is a clear presence of wakes of four different sizes, corresponding to the four fractal iterations of the grid. The interactions between these wakes give rise to the wake interaction length scale

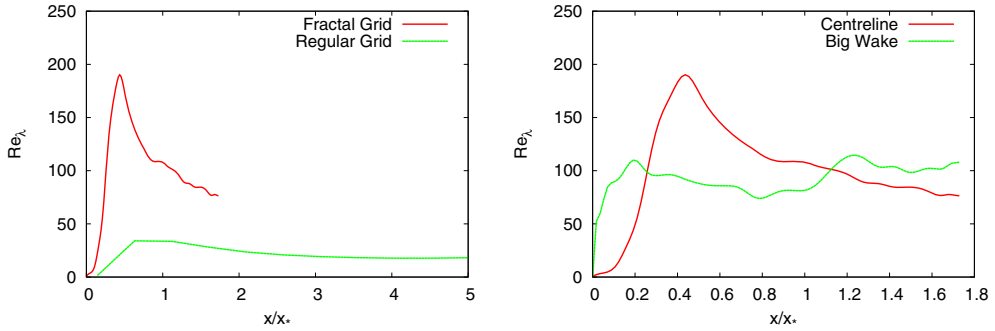

Figure 4. (Left) Centreline Re_λ as functions of streamwise coordinate normalized by the wake-interaction length scale x_*. (Right) Re_λ versus x/x_* along the centreline of the fractal grid and along a line normal to the fractal grid and crossing its biggest bar at the middle.

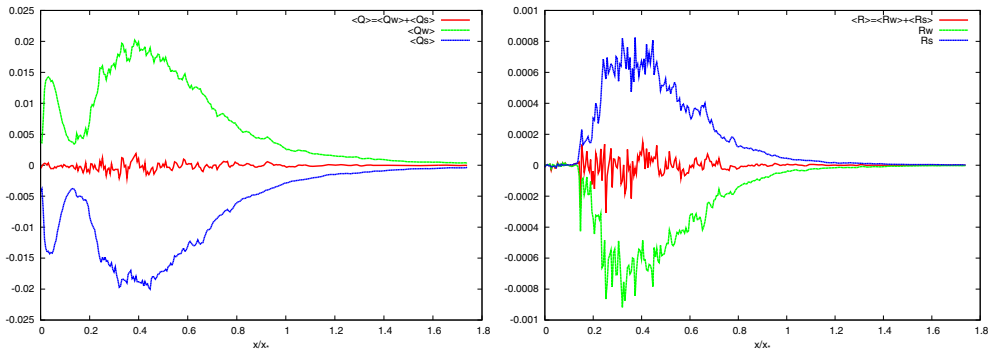

Figure 5. Plots along the centreline for the fractal grid. (a) Q_w, Q_s and Q as functions of x/x_*. (b) R_w, R_s and R as functions of x/x_*.

x_* introduced, generalized and discussed by Mazellier and Vassilicos (2010) and Gomes-Fernandes *et al* (2012). As shown by these studies, the wake interaction length scale is appropriate for scaling the downstream development of grid-generated turbulence along the centreline. In figure 4(a) we plot Re_λ as a function of x/x_* along the centreline of both the regular and the fractal grid-generated turbulent flows. This local Reynolds number peaks close to $0.4x_*$ or $0.5x_*$ for both flows, although not at exactly the same point. The value of Re_λ is everywhere below 40 for the regular grid but reaches above 150 for the fractal grid. In figure 4(b) we plot the development of Re_λ along two different streamwise straight lines. In view of the much higher Reynolds numbers achieved by the fractal grid along the centreline, we concentrate our attention on fractal grid results in the remainder of this paper.

Defining $Q_w \equiv \frac{1}{4}\omega^2$, $Q_s \equiv -\frac{1}{2}s_{ij}s_{ij}$, $R_w \equiv -\frac{1}{4}\omega_i\omega_j s_{ij}$ and $R_s \equiv -\frac{1}{3}s_{ij}s_{jk}s_{ki}$, in figure 5 we plot $\langle Q_w\rangle$, $\langle Q_s\rangle$ and $\langle Q\rangle = \langle Q_w + Q_s\rangle$ as functions of x/x_* as well as $\langle R_w\rangle$, $\langle R_s\rangle$ and $\langle R\rangle = \langle R_w + R_s\rangle$ as functions of x/x_* along the centreline for the fractal grid. Firstly, we note that $\langle Q\rangle = 0$ and $\langle R\rangle = 0$ throughout the domain along the centreline. This is not a trivial result because this turbulence is not homogeneous, particularly at $x < x_*$ (see Seoud *et al* 2007, Mazellier and Vassilicos 2010, Laizet and Vassilicos 2011, Valente and Vassilicos 2011). Secondly, we note the remarkable region $0 < x/x_* < 0.16$ where $\langle R_w\rangle = \langle R_s\rangle = 0$ but $\langle Q_w\rangle$ and $\langle Q_s\rangle$ are not zero. Then something happens around $x/x_* \approx 0.16$ which

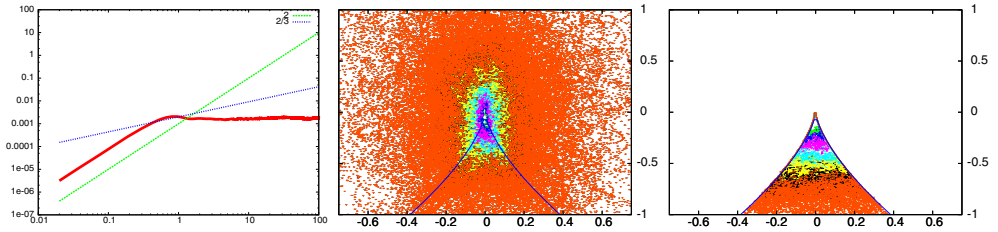

Figure 6. (a) $\langle \delta u^2(\tau) \rangle / U_\infty^2$ versus $\tau U_\infty / t_{\min}$, (b) Q–R diagram and (c) Q_s–R_s diagram at $x/x_* = 0.052$.

sets off non-zero values of average enstrophy and strain-rate production rates. At this point, $\langle R_w \rangle$ and $\langle R_s \rangle$ start growing in magnitude (with opposite signs to keep $\langle R \rangle = 0$) and reach a peak where the local Reynolds number peaks (see figure 4). $\langle Q_w \rangle$ and $\langle Q_s \rangle$ peak at the same point. Further downstream, $\langle R_w \rangle$, $\langle R_s \rangle$, $\langle Q_w \rangle$, $\langle Q_s \rangle$ and Re_λ continuously decay together.

The negative sign of $\langle R_w \rangle$ throughout the region where it is non-zero implies positive enstrophy production which would imply a creation of increasingly small scales (perhaps a cascade of sorts) in the sense that fluctuating velocity derivatives on average increase. No such behaviour seems to exist in the region $0 < x/x_* < 0.16$. The increase and then decrease of enstrophy along the centreline in this region may have to do with enstrophy being advected from nearby and then left to decay as it is swept downstream for as long as enstrophy production has not yet started.

There seems to be a flow phenomenon here which triggers a sudden production of increasingly small-scale velocity fluctuations at a finite distance from the inlet. The picture suggested in section 2 is one where a flow phenomenon occurs near the inlet and causes a wide separation between inner and outer scales, which, in turn, causes some kind of cascade. This cascade persists for a significant distance downstream similarly to the centreline positive production of enstrophy which is initiated near $x/x_* = 0.16$ and which persists for as long downstream as our simulation goes. To complete the parallels with the picture of section 2 we now need to find where the range of scales is greatest in fractal-generated turbulent flow along the centreline and where it is initiated. The scale-range diagnostic we use for this task is the second-order structure function in time, i.e. $\langle \delta u^2(\tau) \rangle$ where $\delta u(\tau) = u(x,t) - u(x,t+\tau)$ in terms of the streamwise fluctuating component $u(x,t)$ at point x on the centreline at time t. The average defining $\langle \delta u^2(\tau) \rangle$ is taken over time; and $\langle \delta u^2(\tau) \rangle$ is a function of x and τ.

We now document the downstream development of $\langle \delta u^2(\tau) \rangle$ in parallel with a documentation of the downstream development of the Q–R diagram. It is of interest to see how the Q–R diagram obtains its tear-drop shape which is suspected by some authors to be universal (Tsinober 2009). Figures 6–19 provide plots of $\langle \delta u^2(\tau) \rangle / U_\infty^2$ versus $\tau U_\infty / t_{\min}$ and Q–R diagrams at different positions x/x_* along the centreline. The vertical/horizontal axes on the Q–R diagrams are for $Q/\langle \mathrm{tr}(\mathbf{s}^2) \rangle$ and $R/\langle \mathrm{tr}(\mathbf{s}^2) \rangle^{3/2}$, respectively, and the plot is of isocontours of the probability density function of (Q, R), statistics having been taken over time. We also report Q_s–R_s diagrams normalized in the same way as our Q–R plots. Values of the $(Q_s$–$R_s)$ pair always fall under the zero-discriminant line $\frac{27}{4} Q_s^3 + R_s^2 = 0$ in the Q_s–R_s diagram simply because Q_s and R_s are the second and third invariants of the strain-rate tensor which is a real symmetric matrix.

The main observation to make from these figures is that, towards the end of the region in which there is no vortex stretching and no positive production of enstrophy, quite suddenly $\langle \delta u^2(\tau) \rangle$ adopts a well-defined power-law shape over more than a decade with a scaling

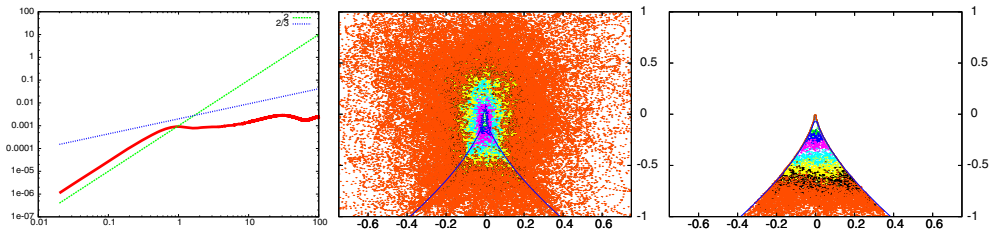

Figure 7. (a) $\langle \delta u^2(\tau) \rangle / U_\infty^2$ versus $\tau U_\infty / t_{\min}$, (b) Q–R diagram and (c) Q_s–R_s diagram at $x/x_* = 0.105$.

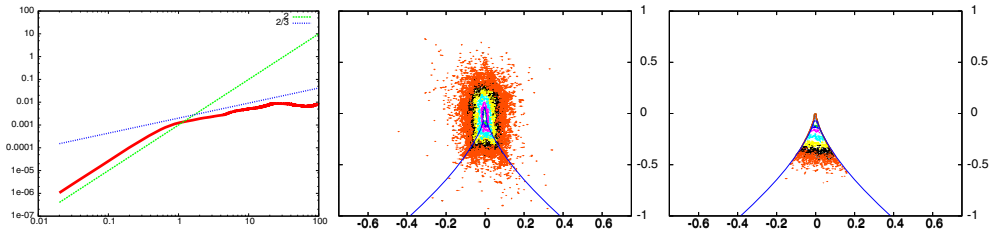

Figure 8. (a) $\langle \delta u^2(\tau) \rangle / U_\infty^2$ versus $\tau U_\infty / t_{\min}$, (b) Q–R diagram and (c) Q_s–R_s diagram at $x/x_* = 0.157$.

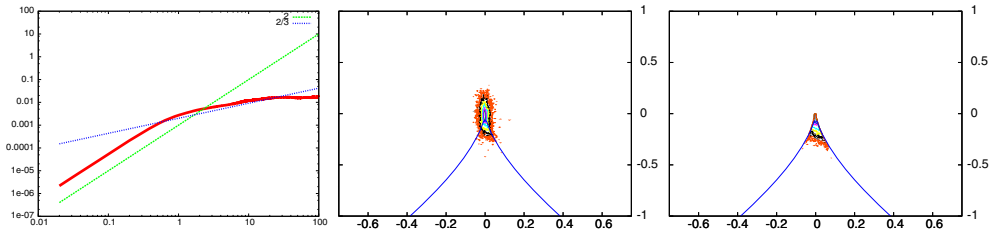

Figure 9. (a) $\langle \delta u^2(\tau) \rangle / U_\infty^2$ versus $\tau U_\infty / t_{\min}$, (b) Q–R diagram and (c) Q_s–R_s diagram at $x/x_* = 0.210$.

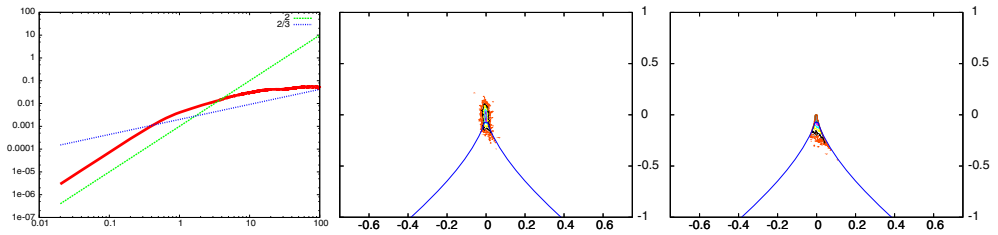

Figure 10. (a) $\langle \delta u^2(\tau) \rangle / U_\infty^2$ versus $\tau U_\infty / t_{\min}$, (b) Q–R diagram and (c) Q_s–R_s diagram at $x/x_* = 0.262$.

exponent very close to 2/3, the very exponent predicted by Kolmogorov for second-order structure functions in space. We leave the discussion concerning the correspondence between structure functions in space and in time for future work and simply concentrate on the fact that, quite clearly, there is a wide power-law range of excited scales at $x/x_* = 0.157$ even though the Q–R diagram has not yet adopted its tear-drop shape and the production rates of

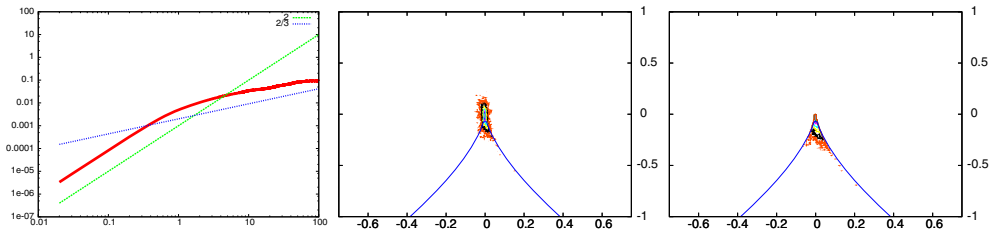

Figure 11. (a) $\langle \delta u^2(\tau) \rangle / U_\infty^2$ versus $\tau U_\infty / t_{\min}$, (b) Q–R diagram and (c) Q_s–R_s diagram at $x/x_* = 0.315$.

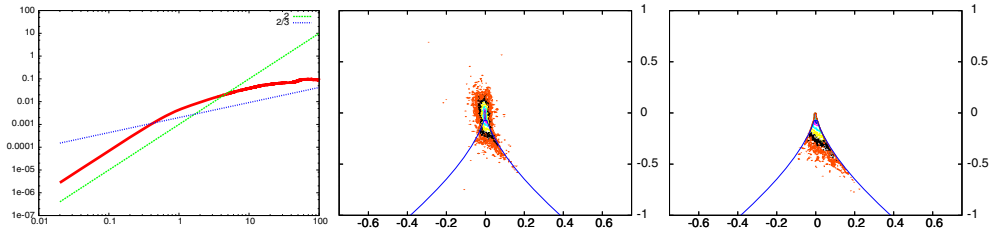

Figure 12. (a) $\langle \delta u^2(\tau) \rangle / U_\infty^2$ versus $\tau U_\infty / t_{\min}$, (b) Q–R diagram and (c) Q_s–R_s diagram at $x/x_* = 0.367$.

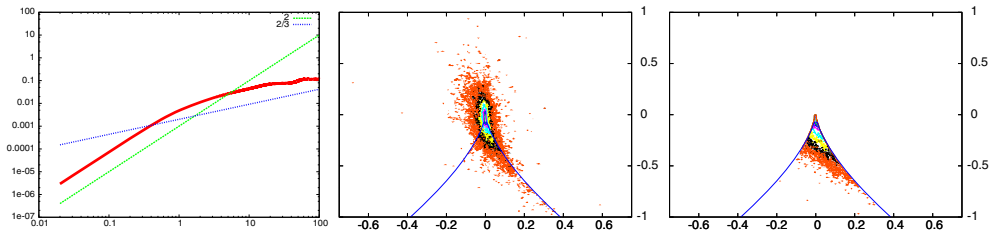

Figure 13. (a) $\langle \delta u^2(\tau) \rangle / U_\infty^2$ versus $\tau U_\infty / t_{\min}$, (b) Q–R diagram and (c) Q_s–R_s diagram at $x/x_* = 0.420$.

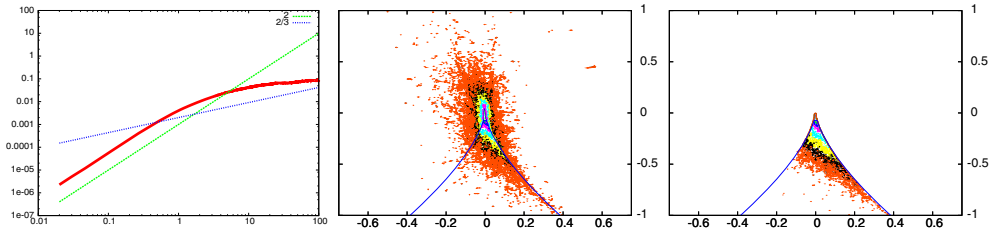

Figure 14. (a) $\langle \delta u^2(\tau) \rangle / U_\infty^2$ versus $\tau U_\infty / t_{\min}$, (b) Q–R diagram and (c) Q_s–R_s diagram at $x/x_* = 0.525$.

enstrophy and strain rate are both zero. It is remarkable that the local Reynolds number Re_λ is only about 30 at $x/x_* = 0.157$. We mention here that such a behaviour was observed neither on the centreline of the regular grid nor along a line normal to the fractal grid and crossing its biggest bar at the middle. Note that in the regular grid case, the centreline crosses one of the grid's bars, so there may be an important distinction to be made between being inside a wake

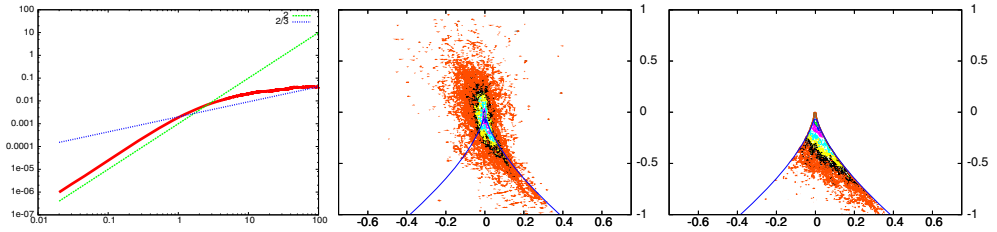

Figure 15. (a) $\langle \delta u^2(\tau) \rangle / U_\infty^2$ versus $\tau U_\infty / t_{\min}$, (b) Q–R diagram and (c) Q_s–R_s diagram at $x/x_* = 0.735$.

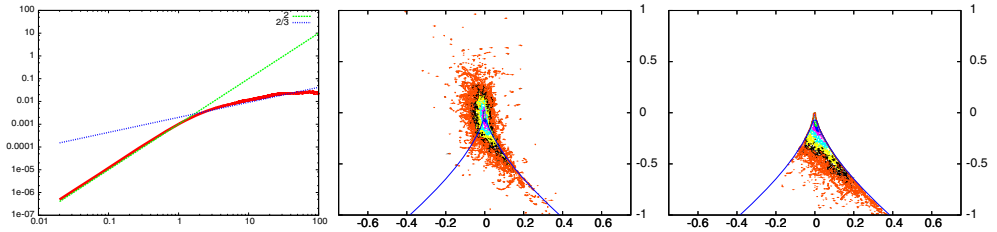

Figure 16. (a) $\langle \delta u^2(\tau) \rangle / U_\infty^2$ versus $\tau U_\infty / t_{\min}$, (b) Q–R diagram and (c) Q_s–R_s diagram at $x/x_* = 0.893$.

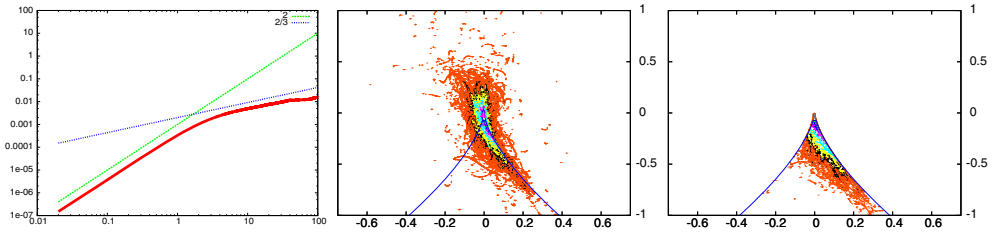

Figure 17. (a) $\langle \delta u^2(\tau) \rangle / U_\infty^2$ versus $\tau U_\infty / t_{\min}$, (b) Q–R diagram and (c) Q_s–R_s diagram at $x/x_* = 1.208$.

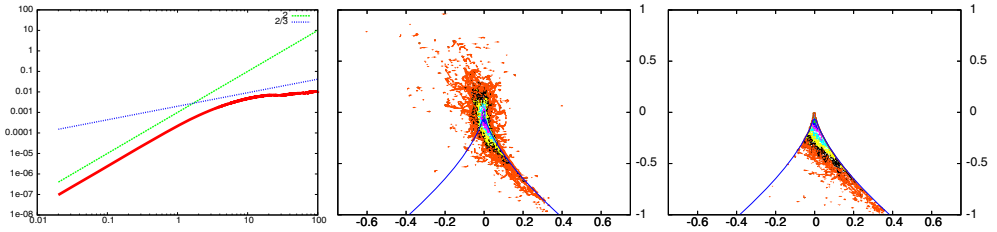

Figure 18. (a) $\langle \delta u^2(\tau) \rangle / U_\infty^2$ versus $\tau U_\infty / t_{\min}$, (b) Q–R diagram and (c) Q_s–R_s diagram at $x/x_* = 1.366$.

of a bar or in a region between wakes. This is also a potentially important point which will need a careful and detailed study in the future.

The Q_s–R_s diagram acquires its well-known shape (e.g. Soria *et al* 1994) favouring positive values of R_s and negative values of Q_s just under the zero-discriminant line $\frac{27}{4} Q_s^3 + R_s^2 = 0$ only progressively and after the appearance of the 2/3 power law for $\langle \delta u^2(\tau) \rangle$.

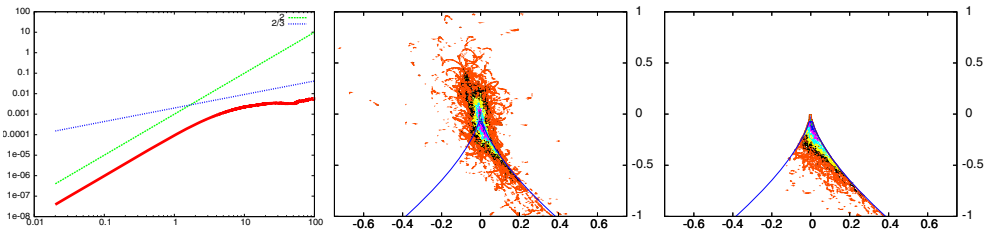

Figure 19. (a) $\langle \delta u^2(\tau) \rangle / U_\infty^2$ versus $\tau U_\infty / t_{\min}$, (b) Q–R diagram and (c) Q_s–R_s diagram at $x/x_* = 1.733$.

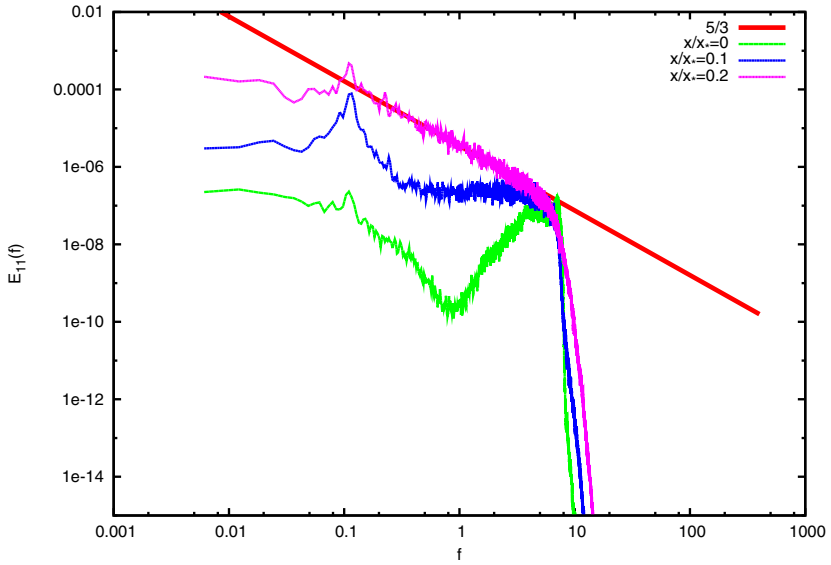

Figure 20. Energy spectra in the frequency domain at different $x/x_* = 0.0, 0.1$ and 0.2. Frequencies are non-dimensionalized by $U_\infty / t_{\min}$ on the horizontal axis. The same simulation as for figures 4(b) and 5–19 but run for ten times more time steps so as to collect ten times more data.

This agrees with our observation that the Q–R diagram also acquires its well-known tear-drop shape progressively after the appearance of this $2/3$ power law quite close to the grid where the local Reynolds number is still low. Clearly, the sequence of events reported in figures 6–19 bears some resemblance to the picture which emerged from the analysis in section 2.

We close this section with some final observations concerning the very near-field region $0 \leqslant x/x_* \leqslant 0.2$ along the centreline of the fractal grid-generated turbulent flow. Figure 20 is a plot of energy spectra (in the frequency domain) at three very near-field positions, $x/x_* = 0$, $x/x_* = 0.1$ and $x/x_* = 0.2$ on the centreline. In agreement with figures 8(a) and 9(a), the energy spectrum exhibits a well-defined $-5/3$ power-law shape over between one and two decades at $x/x_* = 0.2$ even though the local Re_λ is only about 30 at this point! At $x/x_* = 0$, however, the energy spectrum is dominated by two excited frequencies, one being the shedding frequency of the big bar wakes and the other characterizing the secondary instability of the shear layers. These frequencies differ by a factor of about 40 which is comparable with $Re_{\mathrm{I}}^{\beta/2} Re_{\mathrm{L}}^{(1-\alpha)/2}$ if $\beta = \alpha = 1$ as in Valente and Vassilicos (2012). The range over which the $-5/3$ spectrum develops is determined by these two frequencies rather than by Re_λ and

its extent is set by their ratio 40. This is therefore a spectrum where the range of length scales is directly set by inlet conditions and does not obviously relate to Kolmogorov scalings. The spectrum then develops its $-5/3$ power-law shape within this pre-determined range of frequencies. There are analogies here with our results of section 2 even though they concern a different type of flow.

5. Conclusion

We have shown under assumptions 1 and 2 in section 2 that, for decaying homogeneous turbulence, a wide range of wavenumbers exists where the interscale energy flux depends on inlet/initial Reynolds number, is negative (kinetic energy is on average transferred from small to high wavenumbers) and is independent of wavenumber but not necessarily of viscosity. The picture that seems to emerge from these assumptions is that something may be happening near the inlet/initial conditions causing assumption 2 to materialize, which then, if the inlet/initial Reynolds number is large enough, immediately triggers the existence of a wide range of wavenumbers. The very existence of two widely separated, one large and one small, length scales then gives rise itself to an average energy cascade down the scales at a rate ϵ. This cascade persists for as long as the local Reynolds number $Re_{\mathrm{L}}(t)$ is large enough to keep $Re_{\mathrm{L}}(0)^{\beta/2} Re_{\mathrm{L}}^{(1-\alpha)/2} \gg 1$ and it is such that the interscale energy flux is independent of wavenumber but not necessarily of viscosity. Unlike the usual Richardson–Kolmogorov cascade, this flux depends on inlet/initial conditions through its dependence on $Re_{\mathrm{L}}(0)$ or Re_{I}.

We then presented results from a DNS of fractal-generated turbulence. We found that $\langle Q \rangle = 0$ and $\langle R \rangle = 0$ throughout the domain along the centreline, which is not trivial as the turbulence is not homogeneous, particularly at $x < x_*$ (see Seoud *et al* 2007, Mazellier and Vassilicos 2010, Laizet and Vassilicos 2011, Valente and Vassilicos 2011). In the centreline region $0 < x/x_* < 0.16$, $\langle R_w \rangle = \langle R_s \rangle = 0$ even though $\langle Q_w \rangle$ and $\langle Q_s \rangle$ are not zero. Close to the end of this near-field centreline region the second-order structure function in time exhibits a well-defined $2/3$ power-law over more than a decade even though the local Reynolds number Re_λ is only about 30. Then something happens around $x/x_* \approx 0.16$ which sets off non-zero values of average enstrophy and strain-rate production rates, and $\langle R_w \rangle$ and $\langle R_s \rangle$ start growing in magnitude with centreline downstream distance (with opposite signs so as to keep $\langle R \rangle = 0$). These two quantities as well as $\langle Q_w \rangle$ and $\langle Q_s \rangle$ reach a peak where the local Reynolds number peaks (see figure 4). Further downstream, $\langle R_w \rangle$, $\langle R_s \rangle$, $\langle Q_w \rangle$, $\langle Q_s \rangle$ and Re_λ continuously decay together.

The Q–R and Q_{s}–R_{s} diagrams do not have their usual appearance in the centreline region $0 < x/x_* < 0.16$ but develop it gradually as the flow progresses downstream and the wide $2/3$ power law of the second-order structure function is eroded.

This work highlights areas requiring future investigation. Assumption 1b needs to be assessed by future laboratory and computational data as there are important consequences if it is not true. It is also important to study structure functions in space and their relations to structure functions in time. These two avenues of research are related as they both touch upon two-point statistics in space and require a dedicated study. Equally if not even more important will be the study of the near-field region $0 < x/x_* < 0.16$ and the investigation of the flow phenomena/instabilities responsible for the rather unexpected properties that we have observed there. We are currently working along these directions and hope to be able to report in the not too distant future.

Acknowledgments

We are grateful to Dr Ryo Onishi for kindly providing us with his data for figure 2. We also acknowledge support from EPSRC research grant number EP/H030875/1.

References

Batchelor G K 1953 *The Theory of Homogeneous Turbulence* (Cambridge: Cambridge University Press)

Discetti S, Ziskin I B, Astarita T and Adrian R J 2013 PIV measurements of anisotropy and inhomogeneity in decaying fractal generated turbulence *Fluid Dyn. Res.* **45** 061401

Frisch U 1995 *Turbulence* (Cambridge: Cambridge University Press)

George W K 1992 The decay of homogeneous isotropic turbulence *Phys. Fluids* A **4** 1492–509

Gomes-Fernandes R, Ganapathisubramani B and Vassilicos J C 2012 PIV study of fractal-generated turbulence *J. Fluid Mech.* **701** 306–36

Hurst D and Vassilicos J C 2007 Scalings and decay of fractal-generated turbulence *Phys. Fluids* **19** 035103

Laizet S and Lamballais E 2009 High-order compact schemes for incompressible flows: a simple and efficient method with the quasi-spectral accuracy *J. Comput. Phys.* **228** 5989–6015

Laizet S and Li N 2011 Incompact3d, a powerful tool to tackle turbulence problems with up to $0(10^5)$ computational cores *Int. J. Numer. Methods Fluids* **67** 1735–57

Laizet S and Vassilicos J C 2011 DNS of fractal-generated turbulence *Flow Turbul. Combust.* **87** 673–705

Laizet S and Vassilicos J C 2012 The fractal space-scale unfolding mechanism for energy-efficient turbulent mixing *Phys. Rev.* E **86** 046302

Lundgren T S 2002 Kolmogorov two-thirds law by matched asymptotic expansion *Phys. Fluids* **14** 638–43

Lundgren T S 2003 Kolmogorov turbulence by matched asymptotic expansions *Phys. Fluids* **15** 1074–81

Mazellier N and Vassilicos J C 2010 Turbulence without Richardson–Kolmogorov cascade *Phys. Fluids* **22** 075101

Onishi R, Baba Y and Takahashi K 2011 Large-scale forcing with less communication in finite-difference simulations of stationary isotropic turbulence *J. Comput. Phys.* **230** 4088–99

Parnaudeau P, Carlier J, Heitz D and Lamballais E 2008 Experimental and numerical studies of the flow over a circular cylinder at Reynolds number 3900 *Phys. Fluids* **20** 085101

Sagaut P and Cambon C 2008 *Homogeneous Turbulence Dynamics* (Cambridge: Cambridge University Press)

Seoud R E and Vassilicos J C 2007 Dissipation and decay of fractal-generated turbulence *Phys. Fluids* **19** 105108

Soria J, Sondergaard R, Cantwell B J, Chong M S and Perry A E 1994 A study of the fine-scale motions of incompressible time-developing mixing layers *Phys. Fluids* **6** 871–84

Taylor G I 1935 Statistical theory of turbulence *Proc. R. Soc. Lond.* **151A** 421–78

Tchoufag J, Sagaut P and Cambon C 2012 Spectral approach to finite Reynolds number effects on Kolmogorov's 4/5 law in isotropic turbulence *Phys. Fluids* **24** 015107

Tennekes H and Lumley L J 1972 *A First Course in Turbulence* (Cambridge, MA: MIT)

Townsend A A 1956 *The Structure of Turbulent Shear Flows* (Cambridge: Cambridge University Press)

Tsinober A 2009 *An Informal Conceptual Introduction to Turbulence* (Berlin: Springer)

Valente P and Vassilicos J C 2011 The decay of turbulence generated by a class of multi-scale grids *J. Fluid Mech.* **687** 300–40

Valente P and Vassilicos J C 2012 Universal dissipation scaling for non-equilibrium turbulence *Phys. Rev. Lett.* **108** 214503